Review of the U.S. Department of Energy's "Deep Dive" Effort to Understand Voltage Fade in Li- and Mn-rich Cathodes

Jason R. Croy[1,*], Mahalingam Balasubramanian[2], Kevin G. Gallagher[1], and Anthony K. Burrell[1]

[1]Chemical Sciences and Engineering Division, [2]X-ray Science Division, ~~Advanced Photon Source,~~ Argonne National Laboratory, Illinois, 60439, United States

*croy@anl.gov

Conspectus

The commercial introduction of the lithium-ion (Li-ion) battery nearly 25 years ago marked a technological turning point. Portable electronics, dependent on energy storage devices, have permeated our world and profoundly affected our daily lives in a way that cannot be understated. Now, at a time when societies and governments alike are acutely aware of the need for advanced energy solutions, the Li-ion battery may again change the way we do business. With roughly two-thirds of daily oil consumption in the United States allotted for transportation, the possibility of efficient and affordable electric vehicles suggests a way to substantially alleviate the Country's dependence on oil and mitigate the rise of greenhouse gases. Although commercialized Li-ion batteries do not currently meet the stringent demands of a would-be, economically competitive, electrified vehicle fleet, significant efforts are being focused on promising new materials for the next generation of Li-ion batteries.

The leading class of materials most suitable for the challenge is the Li- and manganese-rich class of oxides. Denoted as LMR-NMC (Li-manganese-rich, nickel, manganese, cobalt), these materials could significantly improve energy densities, cost, and safety, relative to state-of-the-art Ni- and Co-rich Li-ion cells, if successfully developed.[1] The success or failure of such a development relies heavily on understanding two defining characteristics of LMR-NMC cathodes. The first is a mechanism whereby the average voltage of cells continuously decreases with each successive charge and discharge cycle. This phenomenon, known as voltage fade, decreases the energy output of cells to unacceptable levels too early in cycling. The second characteristic is a pronounced hysteresis, or voltage difference, between charge and discharge cycles. The hysteresis represents not only an energy inefficiency (i.e., energy in vs. energy out) but may also complicate the state of charge/depth of discharge (SOC/DOD) management of larger systems; especially when accompanied by voltage fade.

In 2012 the United States Department of Energy's Office of Vehicle Technologies, well aware of the inherent potential of LMR-NMC materials for improving the energy density of automotive energy storage systems, tasked a team of scientists across the National Laboratory Complex to investigate the phenomenon of voltage fade. ~~This article gives a brief summary of the findings of that two-year investigation~~. Unique studies using synchrotron X-ray absorption (XAS) and high-resolution diffraction (HR-XRD) were coupled with nuclear magnetic resonance spectroscopy (NMR), neutron diffraction, high-resolution transmission electron microscopy (HR-TEM), first-principles calculations and molecular dynamics simulations, and detailed electrochemical analyses.

These studies demonstrated for the first time the atomic-scale, structure-property relationships that exist between nanoscale inhomogeneities and defects, and the macroscale, electrochemical performance of these layered oxides. These inhomogeneities and defects have been directly correlated with voltage fade and hysteresis and a~~. A~~ model describing these mechanisms has been~~is~~ proposed. ~~and the future prospects of LMR-NMCs are discussed.~~This article gives a brief summary of the findings of this recently-concluded, ~~two~~ ~three-year investigation. The interested reader is directed to the extensive body of work cited in the given references for a more comprehensive review of the subject.

Introduction

xLi_2MnO_3•$(1-x)LiMO_2$ (LMR-NMC, M=Mn, Ni, Co) electrodes can provide reversible capacities >230 mAh/g along with considerable energy densities.[2] As a reference, current Li-ion cathodes typically cycle ~150-180 mAh/g.[3] The source of high capacity for LMR-NMC is the "excess" Li (compared to $LiMO_2$) within the ~~transition metal (TM) layers of the~~ Li_2MnO_3 component. However, in order to access this Li, cells must be charged above ~4.4 V (vs. Li) – a process termed "activation". The activation results in irreversible changes to the oxide structure including oxygen loss and TM migration.[4,5] Subsequent cycles suffer from continuous degradation, decreasing average voltage and, therefore, decreasing energy output from cells. In addition, the aforementioned hysteresis persists throughout the life of the cathode. Figure 1 presents the structures and phenomena of interest herein. If these problems are to be mitigated, and the promise of LMR-NMCs realized, then the structure-property relationships that govern this oxide degradation must first be understood.

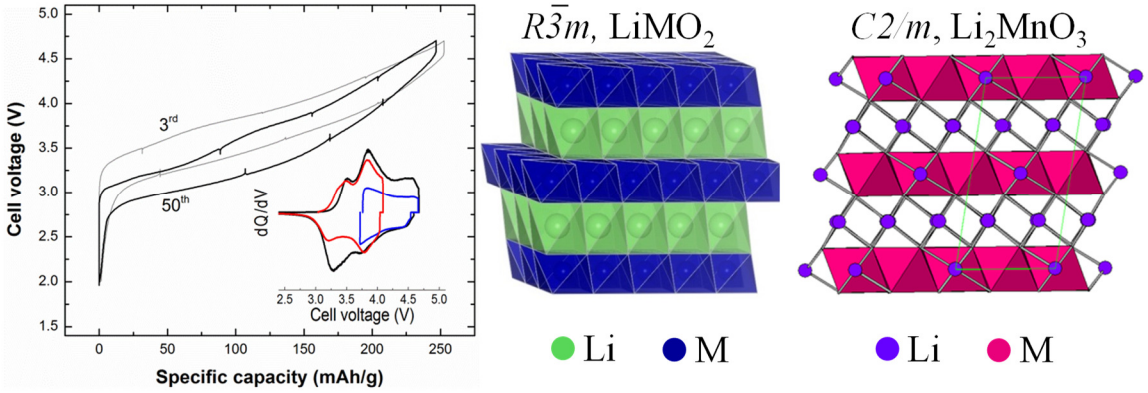

Figure 1 – (*left*) Voltage fade and hysteresis in electrochemical profiles of an LMR-NMC on cycles 3 and 50. Inset shows 3rd-cycle dQ/dVs for cells cycled between 2.0–4.1 V (red), 2.0–4.7 V (black) and 3.7–4.7 V (blue).[15] (*right*) LMR-NMC endmember structures $LiMO_2$ and Li_2MnO_3.

Structure of LMR-NMC

The first problem encountered in deciphering the structure-property relationships of LMR-NMCs is the inherent complexity of the pristine materials themselves. Since their inception there has been significant debate on the structural aspects of these oxides. Namely, "can LMR-NMCs be described as true homogeneous solid solutions, or do they invariably contain nanoscale inhomogeneity, as broadly denoted by the composite notation, xLi_2MnO_3•$(1-x)LiMO_2$?" The heart of the controversy is rooted in the

identification of the long-range symmetry described by diffraction techniques such as XRD. $LiMO_2$ (trigonal, R-3m) and Li_2MnO_3 (monoclinic, C2/m) have compatible oxygen lattices (ccp) allowing an intimate integration of the two structures. In XRD patterns, all R3-m peaks overlap with C2/m peaks except the so-called superstructure peaks that appear at ~23° 2θ [Cu K_α]. These peaks are indexed with respect to C2/m and are a result of cation ordering in the TM layers (e.g., $LiMn_6$) accompanied by the appropriate stacking and coherence along the c-axis.[6] Consequently, all XRD peaks of LMR-NMC can be indexed to the C2/m structure.[7] As such, highly layered and crystalline materials will give diffraction data consistent with the monoclinic structure and have been identified as homogeneous single phase materials. This description of the structure is, however, oversimplified and does not allow important aspects of some structure-property relationships to be ascertained.

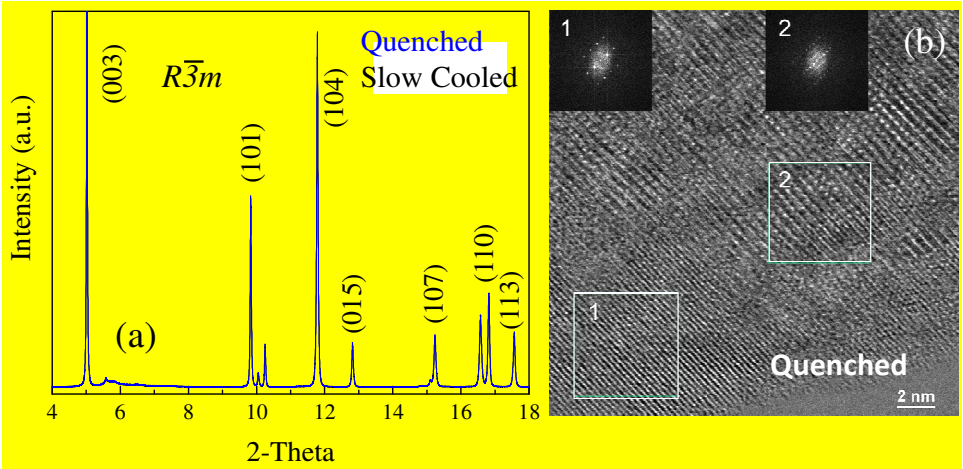

Figure 2 – (a) HR-XRD (λ=0.413893 Å) of $0.5Li_2MnO_3$•$0.5LiCoO_2$ quenched and slow-cooled from 850°C; data sets closely overlap. (b) HR-TEM image of quenched sample showing regions with $LiCoO_2$ (1) and Li_2MnO_3 (2) ordering. Similar results were found for slow-cooled samples.[8]

Figure 2 shows HR-XRD (a) and HR-TEM (b) from $0.5Li_2MnO_3$•$0.5LiCoO_2$ electrode powders quenched (blue) or slow-cooled (black) from 850°C.[8] Both materials are highly crystalline and present well-defined, overlapping HR-XRD peaks [Fig. 2(a)]. The peaks are indexed to R-3m, except the C2/m superstructure peaks that appear at ~5.5° 2θ in the high-resolution data of Fig. 2(a). As discussed, these types of data sets are often interpreted as solid-solution-type structures. However, the HR-TEM data [Fig. 2(b)] highlights regions of two distinct orderings, one similar to $LiCoO_2$ (1) and one similar to Li_2MnO_3 (2).

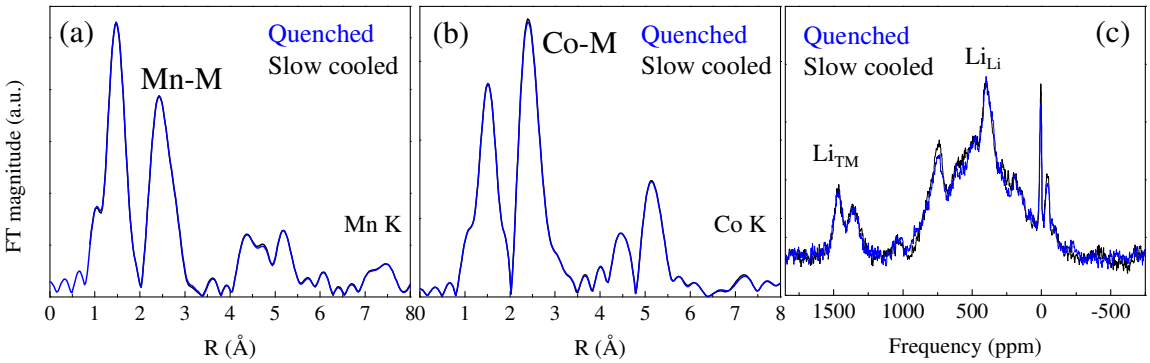

Figure 3 – (a) Mn and (b) Co K-edge EXAFS of $0.5Li_2MnO_3$•$0.5LiCoO_2$ quenched and slow-cooled from 850°C. (c) ^{6}Li NMR of the samples in (a) and (b). Quenched and Slow cooled data sets closely overlap.[8]

Figures 3(a) and (b) show the Mn and Co K-edge, extended X-ray absorption fine structure (EXAFS) data from the $0.5Li_2MnO_3$•$0.5LiCoO_2$ samples of Fig. 2. The respective local environments have not been altered due to synthesis conditions (quenched/slow-cooled) but the differences between the Mn and Co EXAFS data are significant. Analysis of the Co-M (M=Mn/Co) coordination revealed an almost fully coordinated (5.7 ± 0.6) second-shell as would be expected for a layered, R-3m-type oxide. In fact, the Co K-edge EXAFS in Fig. 3(b) bears a strong resemblance to that of pure $LiCoO_2$[9]. Analysis of the Mn-M coordination gives a second-shell coordination of just 3.3 ± 0.7 and reveals a local structure similar to pure Li_2MnO_3 where Li and Mn charge order to create $LiMn_6$ units in the TM layers [see Fig. 5(c)]. Because photoelectron scattering from Li is negligible in the EXAFS experiment, Li in the neighborhood of Mn gives an apparent reduction in nearest-neighbor coordination. These data imply that the excess Li in these materials preferentially orders with Mn in the TM planes[9], consistent with distinct regions in the HR-TEM. While the X-ray data of Figs. 3(a),(b) give a picture of the local environments with respect to the TMs, Fig. 3(c) shows NMR data which directly probes the local structure from the Li-site point of view. The peaks labeled Li_{TM} (~1250–1500 ppm) are signatures of $LiMn_6$ units in the TM planes and also appear in pure Li_2MnO_3[10]; confirming that the excess Li is ordered with Mn. The combined EXAFS, HR-TEM, and NMR data unambiguously identify two distinct environments; one rich in Li and Mn with a local structure similar to Li_2MnO_3, and one rich in TMs with a local structure similar to $LiCoO_2$. The fact that both data sets (quenched/slow-cooled) are similar reveals that the driving force for distinct domain formation is related to the strong tendency for Li^+ and Mn^{4+} to charge order. This ordering is also clear in more complex compositions[2,17] and is likely related to the low onset temperature for Li-Mn ordering, even in pure Li_2MnO_3. [11,12] Consequently, xLi_2MnO_3•$(1-x)LiMO_2$ compositions, particularly those with high x values, show two distinct environments. One, rich in Li and Mn, consists of numerous $LiMn_6$ units within the TM layers and is denoted as the "Li_2MnO_3 component". The other, rich in TMs, consists of highly coordinated TMs with $LiMO_2$ with a $LiMO_2$-type motif ~~ordering;~~ where NiO-like rocksalt domains are possible for certain compositions. We note that NMR data shows disordered Li-regions that do not agree with the pure end-members exclusively.[8] This suggests that coherency strain at the interface is perhaps largely accommodated by distorting the nearby Li sites. These sites might be expected to play a unique role in the electrochemistry. The recognition of distinctly different local

environments in LMR-NMCs, *irrespective of the long-range crystallography that determines the average structure*, is critical and marks a substantial turning point in the effort to understand the mechanisms of voltage fade and hysteresis in LMR-NMC electrodes.

Li_2MnO_3 vs. Li- and Mn-rich Component

As shown above, the local structures of the Li- and Mn-rich domains are similar to pure Li_2MnO_3. However, because of the intimate integration of these domains, simply evoking "Li_2MnO_3" as a pure component does not adequately reflect the material

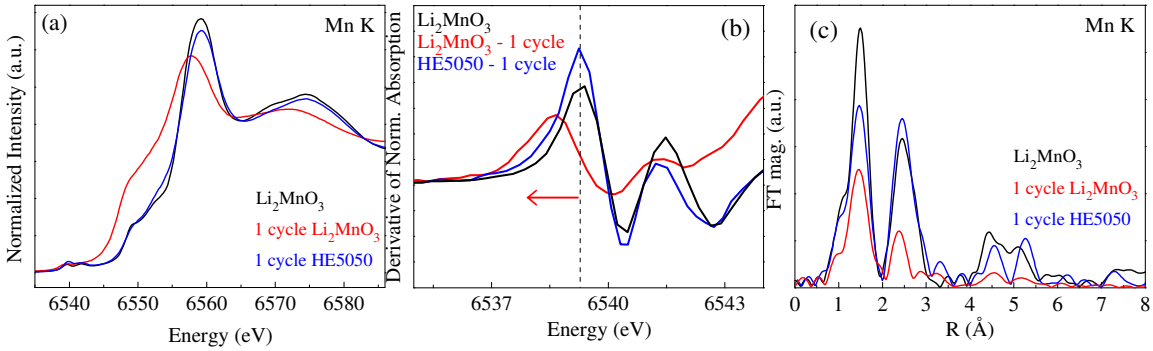

Figure 4 – (a) Mn K-edge XANES of Li_2MnO_3 before (black) and after (red) the first cycle between 5-2.0 V (vs. Li) compared with $0.5Li_2MnO_3$•$0.5LiMn_{0.375}Ni_{0.375}Co_{0.25}O_2$ (HE5050). (b) Derivative of the pre-edge region shown in (a). (c) EXAFS data of samples in (a) and (b).[13]

properties. Figures 4(a),(b) show a comparison of Mn K-edge XAS data from bulk, crystalline Li_2MnO_3 before (black) and after (red) the first electrochemical cycle compared with $0.5Li_2MnO_3$•$0.5LiMn_{0.375}Ni_{0.375}Co_{0.25}O_2$ (HE5050, blue) after the first electrochemical cycle.[13] Notable is the drastic shift to lower energy in the Li_2MnO_3 XANES compared to the minor changes in the cycled LMR-NMC. The EXAFS data, Fig. 4(c), reveals severe damping of all peaks for the Li_2MnO_3 after one cycle while only the first-shell, Mn-O correlations are significantly effected for the LMR-NMC. Analysis confirmed that a large fraction of Mn in the discharged Li_2MnO_3 was present as Mn^{3+} in JT-distorted environments while no clear evidence of Mn^{3+} was observed for the discharged composite. In addition, the Mn-O coordination remains ~6 for Li_2MnO_3 at the top of charge while it is observed to decrease along the plateau of LMR-NMC.[14] Furthermore, NMR studies showed no evidence of structural protons for cycled Li_2MnO_3 or LMR-NMC.[15] Therefore, although the Li- and Mn-rich component of LMR-NMC is locally similar to Li_2MnO_3, several major differences exists: 1) the role of oxygen in charge compensation, and changes in local structures, is different in the two materials; 2) Mn reduction from 4+ to 3+ contributes in a significant way to the first-cycle electrochemistry of Li_2MnO_3 but not significantly for LMR-NMCs. Therefore, any understanding of the mechanisms at play in LMR-NMCs must be achieved with a complete picture of the local structure (inhomogeneity, cation ordering, interfaces…) properly accounted for.

Structure-Electrochemical-Properties

To better understand the role of Li-Mn ordering, systematic compositional and electrochemical studies were undertaken.

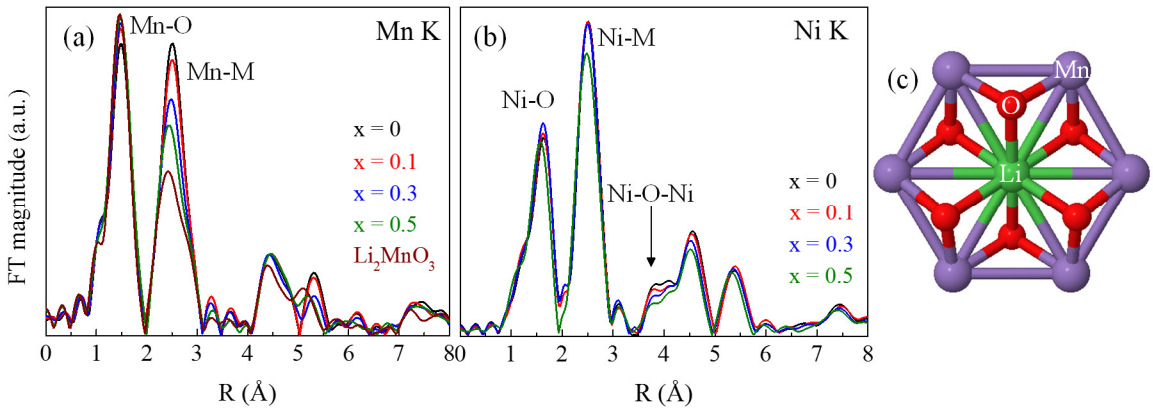

Figure 5 – Mn (a) and Ni (b) K-edge EXAFS of xLi_2MnO_3•(1-x)$LiMn_{0.5}Ni_{0.5}O_2$. (c) $LiMn_6$ unit of pure Li_2MnO_3.[2]

Figure 5(a) shows Mn K-edge EXAFS data of xLi_2MnO_3•(1-x)$LiMn_{0.5}Ni_{0.5}O_2$ electrodes with x=0, 0.1, 0.3, and 0.5.[2] Most evident in the data is the trend of decreasing Mn-M (M=Mn/Ni) correlations with increasing values of x, indicating increasing Li-Mn ordering as previously described. The Ni K-edge EXAFS, Fig. 5(b), shows that the average local environment of Ni is fairly constant with respect to x and is consistent with $LiMO_2$-type structures ~~ordering~~ and the presence of NiO-like structures (e.g., Li/Ni exchange); shown to occur predominately in the Ni- and Mn-rich component.[2]

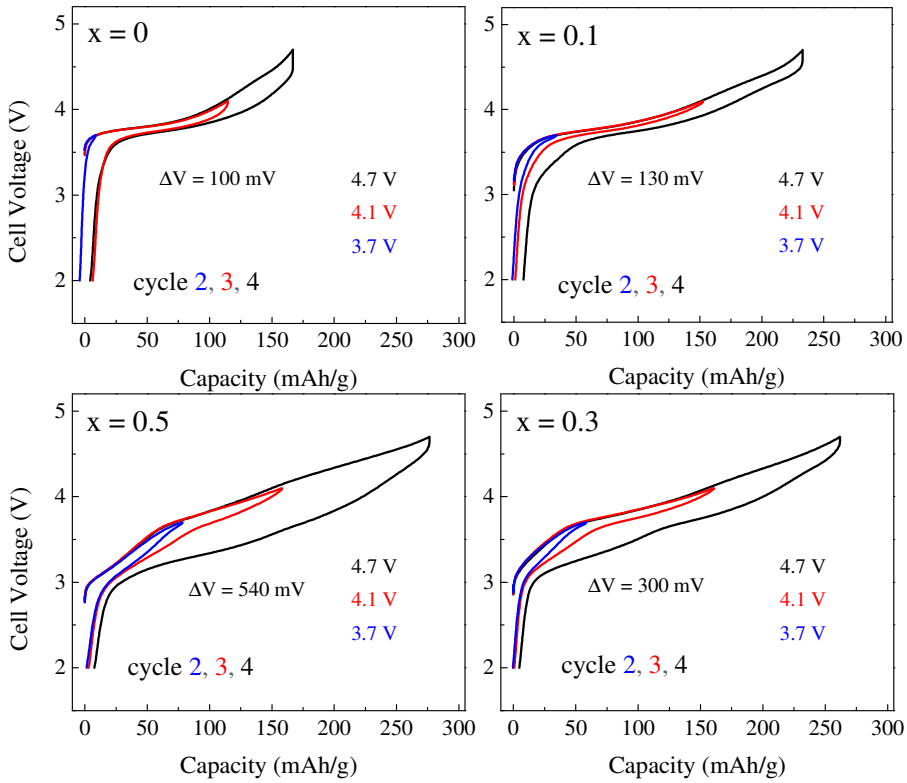

Figure 6 – Consecutive cycles to increasing upper cutoff voltages for xLi_2MnO_3•(1-x)$LiMn_{0.5}Ni_{0.5}O_2$/Li cells. ΔV=magnitude of hysteresis at 50% SOC. All cycles 5 mA/g.[2]

Figure 6 shows electrochemical profiles of the xLi_2MnO_3•$(1-x)LiMn_{0.5}Ni_{0.5}O_2$ series discussed in Fig. 5. The cells were activated between 4.7-2.0 V (5 mA/g, 30°C). Shown in Fig. 6 are consecutive cycles to increasing upper cutoff voltages after the activation cycle. With increasing x there is an increase in the voltage gap between charge and discharge (ΔV). This hysteresis does not occur without the activation process; namely, accessing ~~TM layer~~ the Li associated with the Li_2MnO_3 component. In addition, raising the upper cutoff voltage increases the hysteresis between charge and discharge for x>0. The overlap of the 4.1 V and the 4.7 V cycles for the x=0 composition indicates that the small voltage gap observed may involve other processes than those occurring in the x>0 electrodes.

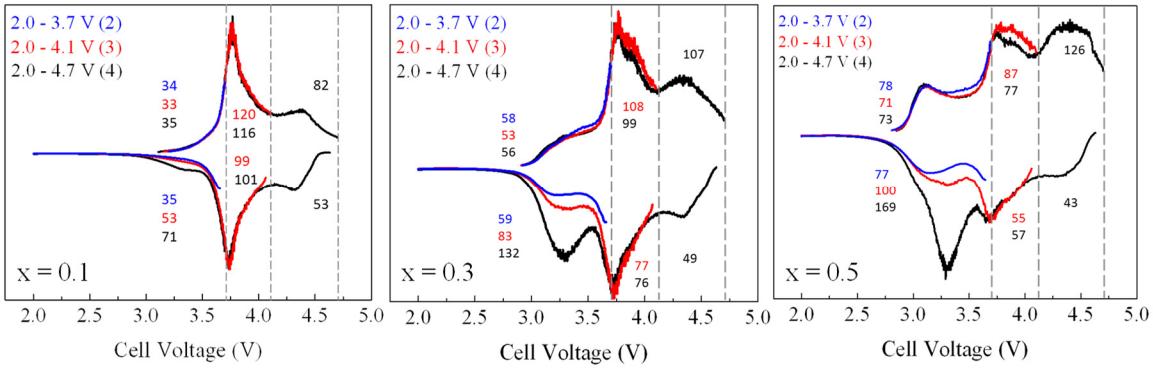

Figure 7 – dQ/dV plots of the window-opening cycles shown in Fig. 6 as described in the text.[2]

Figure 7 shows the associated dQ/dV plots for the profiles in Fig. 6.[2] The numbers along the charge and discharge portions of the dQ/dVs represent the capacities (mAh/g) obtained in the regions (voltage windows) marked by the dashed lines. The numbers and curves are color-coded and labeled (upper left) to match the upper cutoff voltage used. A careful accounting of the capacities in each window reveals that 1) capacities obtained above ~4.0 V on charge cannot be completely re-accommodated until ~3.0 V on discharge. This represents a ~1 V hysteresis for some fraction of the overall Li content. 2) Capacities below ~3.7 V in the charge curves are largely reversible and also increase with increasing x. Similar to hysteresis, this capacity in the low-voltage charge region does not appear unless the Li- and Mn-rich portions of the material are activated. In addition, the capacities in this region grow with cycling and are directly responsible for lowering the average voltages. These studies, combined with the structural data presented so far, ~~illustrate~~ allude to the existence an important structure-property relationship; Li-Mn ordering, and the utilization of the Li from that component, results in both the electrochemical hysteresis and the voltage fade phenomena observed for LMR-NMC electrodes. Furthermore, the magnitude of each is dependent on the extent of Li-Mn ordering. These findings reveal that the underlying mechanisms of voltage fade/hysteresis are closely related.

Figure 8 shows electrochemical cycling of $0.5Li_2MnO_3$•$0.5LiMn_{0.375}Ni_{0.375}Co_{0.25}O_2$/Li cells.[16] The y-axis shows the magnitude of voltage fade over the first ~20 cycles between 4.7-2.0 V. The x-axis shows the lower cutoff voltage used for cycling, where each group of duplicate cells was charged to a fixed upper cutoff of 4.7 V. The dashed line is a guide to the eye and reveals that decreasing the lower cutoff voltage increases the magnitude of

voltage fade. Furthermore, a maximum is seen when cycling over a voltage window of ~4.7-3.2 V. This is the same lower cutoff voltage at which significant Li is reinserted into the structure after charging above ~4.0 V, Fig. 7 (hysteresis). The inset in Fig. 8 shows a calendar time plot of cells cycled in different voltage windows compared to cells that were first activated between 4.7-2.0 V, and then charged to 4.7 V and held constant at that potential (red squares). The y-axis shows the magnitude of voltage fade and the x-axis shows the time on test. Cells that were held constant (4.7 V) clearly show voltage fade from the delithiation at 4.7 V; however, voltage fade in these cells appears to saturate after

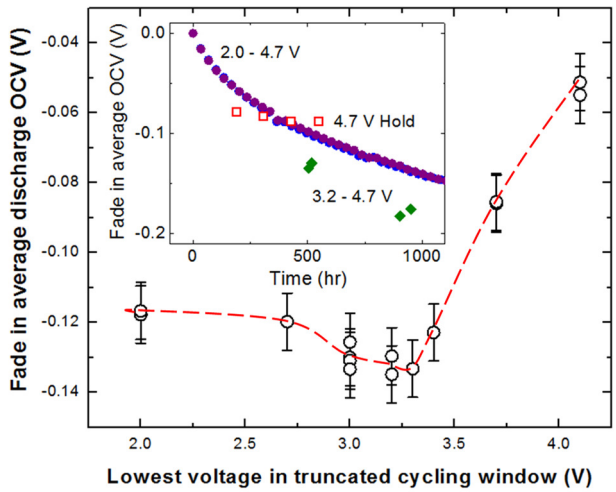

Figure 8 – Cycling window and calendar time plots (insets) for LMR-NMC cells as described in the text. Reprinted from reference (16) with permission from Elsevier.

moderate times. In contrast, cells that were continuously cycled (purple circles, 4.7-2.0 V and green diamonds, 4.7-3.2 V) show a continuous fade with time on test. Furthermore, cycling between 4.7-3.2 V accelerated voltage fade more than any other electrochemical exposure studied. These data show that while high voltage exposure has an effect on voltage fade, actually moving Li in and out of the structure over the voltage window where significant hysteresis occurs plays an important part in the mechanisms that accelerate voltage fade; verifying that voltage fade and hysteresis are correlated.

To gain more insight several X-ray, NMR, and electrochemical studies were conducted.[17,18]

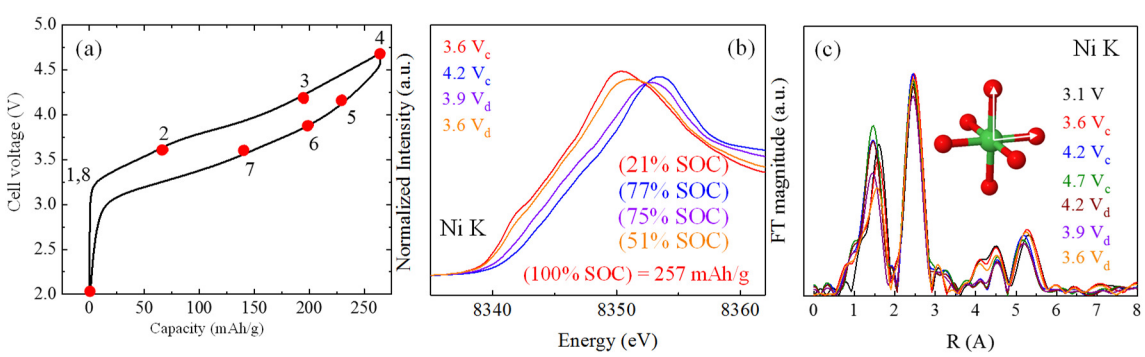

Figure 9 – (a) 7th-cycle charge/discharge for $0.5Li_2MnO_3$•$0.5LiMn_{0.375}Ni_{0.375}Co_{0.25}O_2$/Li cells between 4.7-2.0 V (10 mA/g, 30°C). Red dots indicate example points along the curves at which XAS data were collected. Ni K-edge XANES (b) and EXAFS (c). Inset shows the JT-distorted Ni^{3+} with two distinct Ni-O bond-lengths.[17]

Figure 9(a) shows charge/discharge curves on the 7th cycle, after activation, for $0.5Li_2MnO_3$•$0.5LiMn_{0.375}Ni_{0.375}Co_{0.25}O_2$/Li cells between 4.7-2.0 V. Red dots indicate example points along the curves at which XAS data were collected as shown in (b) and (c). These points represent conditions of equal voltage or equal SOCs and, due to the hysteresis, are not symmetric with respect to charge and discharge. The Ni K-edge XAS in Figs. 9(b) and (c) serve to illustrate the important findings of the study. Namely, even at points of equivalent Li contents (SOCs) the average local structure and oxidation of Ni is different between charge and discharge. This data indicates that Li does not have access to the same sites between charge and discharge, even when the same amount of Li is present in the structure.

High-resolution, magic angle spinning, ^{6}Li solid-state NMR (MAS-NMR) was used to probe these mechanisms from the Li-site point of view[18]. A unique, quantitative analysis was performed via fully-enriched cell components (^{6}Li-enriched metal oxides, electrolytes, and anodes). Tests were performed on activated $0.5^6Li_2MnO_3$•$0.5^6LiMn_{0.5}Ni_{0.5}O_2$ electrodes at similar SOCs as used in the XAS studies, Fig. 10(a). Fig. 10(b) shows NMR data collected during charge and 10(c~~b~~) along discharge corresponding to the points labeled in 10(a). These results show that the last Li sites vacated on charge are not the first sites to be lithiated on discharge. For example, relithiation starts with Li_2MnO_3-like sites at ~710 ppm although Ni-rich environments (≤ 540 ppm) are the first to be delithiated on the previous charge. These data verify the interpretation of the XAS data of ~~, in agreement with XAS data~~Fig. 9 which indirectly imply that lithium does not have access to the same sites between charge and discharge at equivalent SOCs. Additionally, TM-layer Li are found largely removed only at ~4.38 V on charge and are not subsequently reinserted until ~~at least~~ ~3.99~~86~~V on discharge, proving that local Li structures and site occupancies correlate well with the electrochemical hysteresis observed.

A critical observation from these data is the asymmetric, "re-entrant" behavior between charge and discharge of a new process that develops around ~1600 ppm. The intensity of this peak disappears at ~4.4 V on charge [point #3, 10(b)] but does not re-appear until ~3.2 V on discharge [point #7, 10(c)]; in agreement with electrochemical and X-ray studies. Detailed modeling and analysis show that TM-layer Li, coordinated to Mn in tetrahedral sites contribute to the intensities at ~1600 ppm. These data constitute the first, direct observation of these defects in LMR-NMCs.[18] Furthermore, NMR data on repeated cycling shows that this process is only partially reversible and decreases in intensity with subsequent cycles. Quantitative analysis of the ~1600 ppm region indicates that this TM migration and defect site formation involves only 10% of the Li-ions associated with the hysteretic capacity, although a ~1 V hysteresis results.

These important findings show that the hysteresis that develops in LMR-NMC electrodes is structural in nature and results from dynamic changes that occur on a local scale during charge and discharge. It is indubitably clear that the defect chemistry of these complex oxides plays a critical role in their electrochemical and structural behavior.

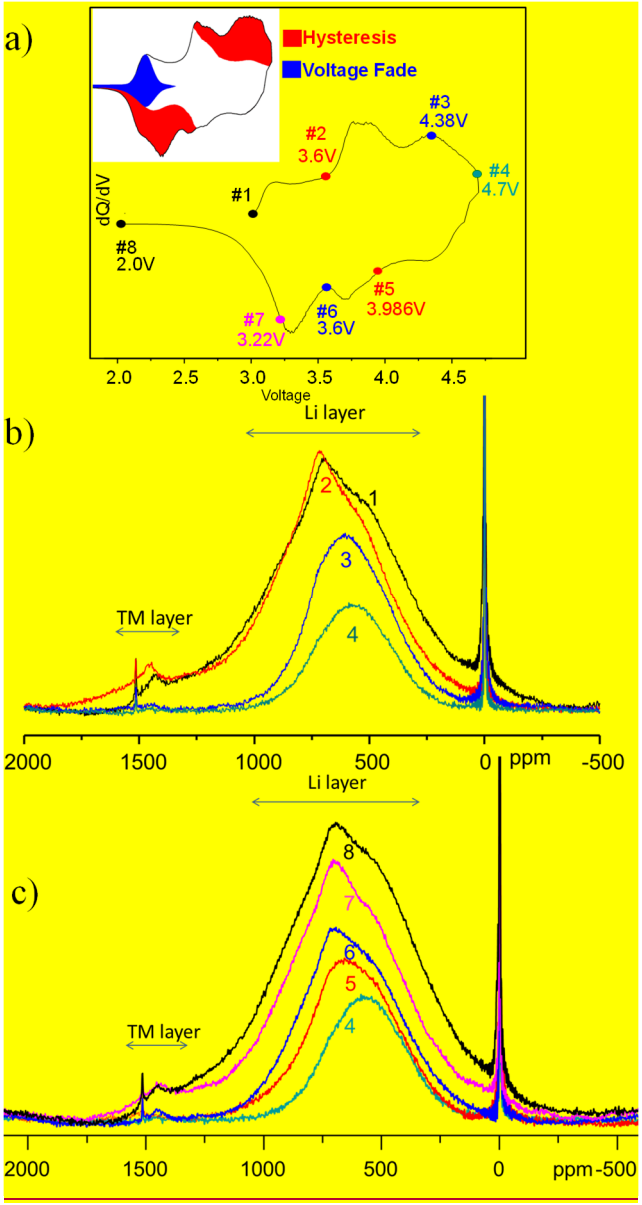

Figure 10 – a) Second-cycle dQ/dV plot labeled corresponding to voltages at which NMR spectra were acquired. Inset shows a~~the~~ schematic representation of hysteresis and voltage fade regions with respect to the dQ/dV shown in a) during second-cycle charge/discharge. b) and c) show ^{6}Li MAS-NMR at various SOCs along the second-cycle charge and discharge, respectively.[18]

Summary of Key Observations

1) The inherent, nanoscale inhomogeneity of LMR-NMCs is driven by charge ordering. Specifically, the strong tendency for Li^{+} and Mn^{4+} to order (e.g., $LiMn_6$) results in two distinct, average local environments, one rich in Li and Mn and the other in TMs.

2) These distinct environments have direct and observable effects on the electrochemical properties of LMR-NMCs that can be tracked during electrochemical cycling. The TM-rich "$LiMO_2$" behaves largely as a standard, layered electrode (e.g., structurally and electrochemically reversible in nature). The Li- and Mn-rich, "Li_2MnO_3" plays a key role

in voltage fade and hysteresis, whereby, accessing Li from this component (activation) triggers the onset of both phenomena. The magnitude of both voltage fade and hysteresis is seen to scale with the magnitude of Li-Mn ordering in as-prepared electrodes.
3) The energetics between charge and discharge are different, even at equivalent Li contents (SOCs), due to local structural differences within electrode particles. This means that Li does not have access to the same sites between charge and discharge at equivalent SOCs. Therefore, the electrochemical hysteresis observed in LMR-NMCs has a structural origin.
4) Voltage fade and hysteresis are correlated. Accessing Li above ~4.0 V causes local structural changes which prohibit the re-accommodation of this Li until ~3.0 V on discharge. Moving Li in and out of the structure (cycling) over this voltage window (e.g., 4.7-3.2 V) accelerates voltage fade more than any other electrochemical exposure studied.

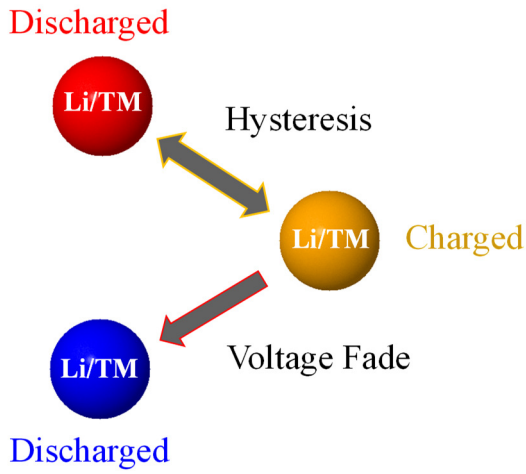

Figure 11 – ~~(a)~~ Schematic of hysteresis/voltage fade mechanism as described in the text. Reprinted from reference (16) with permission from Elsevier.

Model Based on Experimental Observations

Based on the above, key observations, a simple conceptual model has been proposed to describe the hysteresis and voltage fade mechanisms, Fig. 11; however, a more realistic representation of the complex environments and local distortions involved has been derived from calculation (see Fig. 12). Starting with an activated electrode in the discharged state, Li and/or TMs (red) can be induced to migrate once a sufficient SOC is reached on charge. Specifically, once charged beyond ~4.0 V the Li vacancy concentration is high enough to promote Li/TM migration from octahedral sites of the TM layers to tetrahedral sites of the Li-layers and dumbbell-type[19] configurations are formed. More recently, other researchers have reported the presence of transition metals in tetrahedral sites in studies of LMR-NMC materials and other analogous systems.[20-22] Because the tetrahedral sites of the Li layer share faces with three surrounding octahedral Li sites (now vacant due to charging), it is energetically unfavorable to refill these octahedral sites on discharge once the tetrahedral sites are occupied. However, once sufficient Li insertion has occurred on discharge a critical Li content is reached at which point three possibilities may exist:~ 1) The tetrahedral cations are forced to migrate back to their original sites. This process represents a reversible migration at the expense of an

energy penalty paid in the form of a hysteresis. This process, related to the "re-entrant" environments described by NMR, may also explain why there is a minimum in the dashed curve of Fig. 12 where discharging below ~3.2 V may result in more reversibility due to higher driving forces.[23] 2) The cations are forced further along their migration path and come to occupy new sites (e.g., Li-layer octahedral sites). This changes the local structure and lowers the associated Li site energies with respect to further extraction/insertion, thus contributing to voltage fade. 3) Cations can become trapped in the tetrahedral sites of the Li layers. This would be expected to contribute to both capacity loss and impedance rise with extended cycling.

The above processes occur on each charge and discharge cycle where the hysteresis mechanism is reversible for only part of the migrated cations. Cations that migrate to ~~occupy~~ new sites contribute to voltage fade. The model is thus consistent with a slow decay of the hysteresis at the expense of a growing "voltage fade configuration"; that is, the growth of new, local orderings due to the migration of cations from cycle to cycle. This agrees with the NMR and has been verified electrochemically.[2] An appealing aspect of this model is that it equitably explains both hysteresis and voltage fade processes in this class of materials.

First-Cycle Activation

The data and mechanisms discussed so far have been related to "activated" electrodes. However, the mechanisms of hysteresis and voltage fade are set in motion by the processes that occur along the first-cycle plateau. In order to better understand the triggers of cation migration, and to facilitate interpretation of NMR and XAS, atomistic simulations (DFT, GGA+U) were performed. The starting atomic arrangement in the computational unit cell is critical and a bond-pathway analysis method was used to obtain structures consistent with NMR spectra.[24]

To simulate the first cycle, $0.5Li_2MnO_3 \bullet 0.5LiMn_{0.5}Ni_{0.5}O_2$ was considered.[14] A zigzag arrangement of the Ni and Mn ions in $LiMO_2$ stripes was employed. In the first stage of delithiation, Li is removed from the $LiMO_2$ regions at ~4V/Li, on average. During this stage the structure remains intact with only local distortions in response to Li vacancies. In the second stage, half of the Li in the Li layer of the Li_2MnO_3 regions is removed. The structure responds by small, local, atomic displacements while some of the remaining Li migrates to the Li layers. In the next step, the other half of Li in the Li layer of the Li_2MnO_3 regions is removed at ~4.6 V/Li. At this stage, the framework of the structure is destabilized as a result of oxygen oxidation and ions migrate from their original lattice sites to lower their energy. A fraction of the oxygen ions lower their energies through displacements that lead to homopolar O-O bonding with bond-lengths of ~1.3-1.7 Å, indicating the formation of superoxide/peroxide species. Approximately one oxygen for every two Li ions is displaced. The displacement creates oxygen-sublattice vacancies that lower the barrier for Mn migration, and a fraction of the Mn move from the $LiMn_2$ layer to the Li layer. In the resultant structure, the crystalline order of the $LiMO_2$ regions remains mostly intact, while the oxygen sublattice in the Li_2MnO_3 regions becomes highly disordered (Fig. 12). The interfacial region between the stripes is also somewhat affected. A Mn-O (Ni-O) coordination deficit, ΔCN, at the top of the first charge is measured to be ~0.6 for Mn (~0.2 for Ni) using in situ EXAFS, Fig. 13 (a), in reasonable agreement with migrating Mn ions, Fig. 13 (b). Interestingly, the measured ΔCN of Mn

only departs from a value of zero well after the onset of the voltage plateau (marked approximately by the dashed line, Fig. 13). However, the overall behavior is significantly different than pure Li_2MnO_3 ~~discussed above~~ which largely retains a Mn-O coordination of ~6 throughout the first-cycle charge.[12] These observations suggest that oxygen loss and condensation[5] may be the dominant process in Li_2MnO_3 while an additional mechanism – such as the formation of homopolar O-O bonding captured in the MD simulations – may have to be invoked in LMR-NMC, particularly at high states of charge.

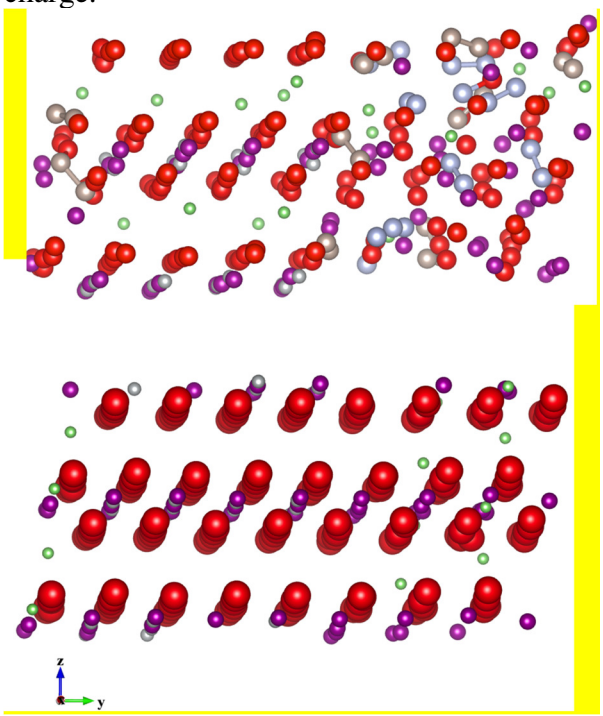

Figure 12 – Atomic structure of $Li_{1/6}Ni_{1/4}Mn_{7/12}O_2$ before (lower panel) and after (upper panel) dynamical simulation at 1000 K for 35 ps. Domain stripes run perpendicular to the plane of projection. The left side of each panel represents the $LiMO_2$ region, and the right side the Li_2MnO_3. Li-green; Ni-grey; Mn-purple; oxygen-red; displaced oxygen forming "free" molecules-blue; displaced oxygen pairs that maintain Mn bonds-brown.[14]

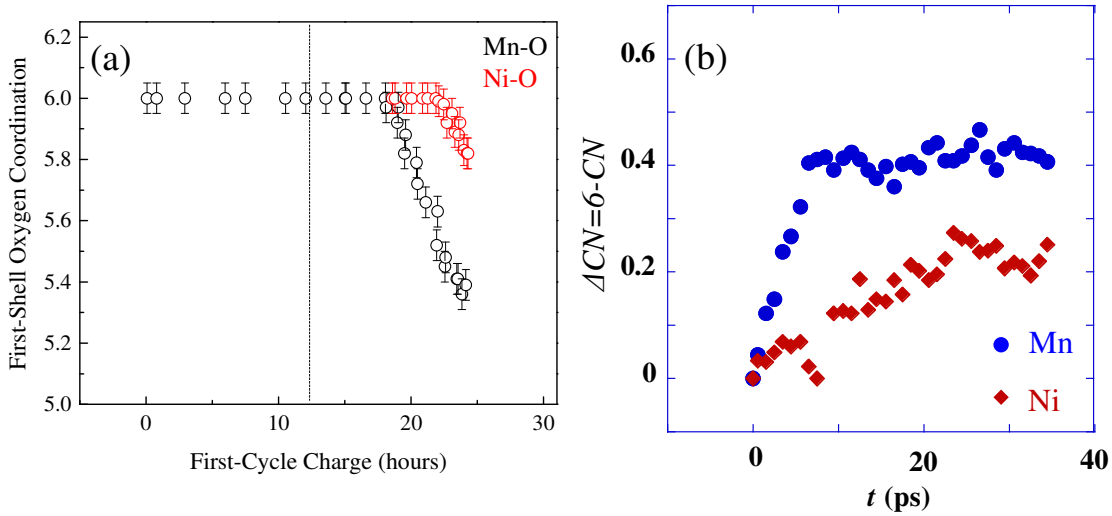

Figure 13 – (a) Changes in Mn/Ni-O coordination (ΔCN) along the first-cycle plateau of $0.3Li_2MnO_3 \bullet 0.7LiMn_{0.5}Ni_{0.5}O_2$ LMR-NMC derived from in situ XAS. The dashed line marks, approximately, the onset of the activation plateau. (b) ΔCN obtained by simulation as described in the text.[14]

Note on the Measurement of Voltage Fade

It is worth re-emphasizing that voltage fade and hysteresis are driven by defects, the concentrations of which are dependent on vacancy concentrations (e.g., Li, O). Moreover, calculations show a predilection for Mn migration in the presence of oxygen vacancies; a consequence of the first-cycle activation. As such, the more Li that is accessed on charge the more prevalent the effects become. Therefore, in studying the effects/mitigation of voltage fade/hysteresis, comparisons should be made among materials that 1) have similar compositions, as it has been shown that Li-Mn ordering, dictated by composition, plays a key role. And 2) similar capacities must be obtained by all samples compared to avoid masking the underlying mechanisms. Many claims have been made that voltage fade can be mitigated by one strategy or another including coatings, synthesis conditions, and dopants/substitutions. However, our extensive research in these areas does not support these claims.[2,17,25-27] In addition, replacing Mn with other, redox active elements, and thereby changing the underlying chemistry, does not correspond to mitigation of voltage fade in LMR-NMCs. In fact, the vast amount of data generated in the last decade related to LMR-NMCs has not produced a single material that does not show some extent of voltage fade and hysteresis, no matter the conditions or strategies presented. The discrepancies, now brought to light by the findings herein, can typically be assigned to biased comparisons, lack of understanding of the fundamental mechanisms, and improper measurement procedures. For example, as voltage fade and hysteresis are driven by vacancy concentrations, comparing various electrodes with large capacity differences, or varying degrees of first-cycle activation, will give misleading results about cycle-life and rates of voltage fade. Moreover, poorly-functioning materials that loose excessive capacity over cycling result in changes in average voltages not related to the mechanisms detailed in this work.

As we are interested in changes in the open-circuit voltage function, impedance effects that can mask changes in voltage profiles must be accounted for to obtain reliable electrode voltages. A ~~universal~~ simple yet important protocol has been developed/implemented to more accurately compare characteristics among various LMR-NMCs. This protocol also makes it straightforward to compare results from different researchers and institutions. Details can be found in reference.[28] Briefly, the protocol consists of a 10 mA/g activation cycle between 4.7-2.0 V (vs. Li/Li^+) to ensure full wetting and activation of the oxide. Subsequent cycles are at 20 mA/g over the same voltage window to ensure a large quantity of Li may be accessed during lithiation/delithiation. Cycling faster reduces the accessible capacity and thus slows the voltage fade mechanism on a per cycle basis. Ageing cycles contain 10-minute current interrupts at several points along charge/discharge from which cell resistances are estimated. Using these values, "iR-corrected" cell voltages can be obtained for charge/discharge cycles. Figure 14 illustrates the difference between measured and iR-corrected charge/discharge voltages where the gap between these two values can vary with cycling and cathode composition. Although seemingly simple in nature, adoption of this standard test has shed light on the importance of one-to-one comparisons of LMR-

NMCs and the vacancy-dependent mechanisms underlying their degradation. We urge other researchers in the field to take these results into consideration in the course of their own electrochemical analyses of LMR-NMCs.

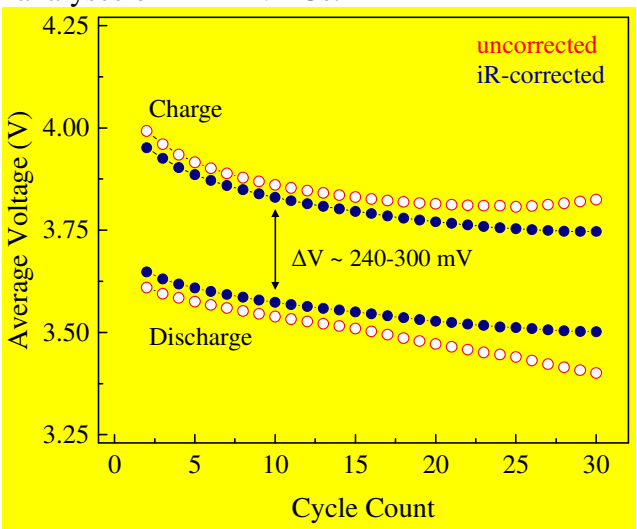

Figure 14 – LMR-NMC cycling data demonstrating the difference between uncorrected (open circles) and iR-corrected (closed circles) average voltages.[28]

Summary

This report summarizes the important findings of a "Deep Dive" effort into the mechanisms of voltage fade and hysteresis associated with xLi_2MnO_3•$(1-x)LiMO_2$, LMR-NMC, cathode materials. It has been shown that irrespective of the long-range crystallography, nanoscale structural inhomogeneity, driven primarily by charge ordering, results in distinct local structures that gives rise to Li- and Mn-rich and TM-rich regions; each of which plays a unique role in the electrochemistry of LMR-NMCs. Notably, the "activation" of the Li- and Mn-rich component, heavily correlated to oxygen involvement along the first-cycle plateau, enables the mechanisms of partially reversible cation migrations during subsequent charge/discharge cycles. These mechanisms involve dynamic structural changes on a local scale and result in the observed hysteresis and the correlated voltage fade; processes which are fundamental to this class of layered materials when accessing Li above ~4.0 V. These studies also implicate defect chemistry in the overall electrochemical behavior of this class of oxides and emphasize the fundamental level at which these issues should be addressed.

As for the future of LMR-NMCs, this class of oxides, despite the challenges, represents one of the few options in cathode materials for achieving significant overall gains with respect to typical $LiMO_2$ and other systems that are considered beyond Li-ion.[1,3] Finally, it is likely that the mechanisms elucidated herein are, at some level, general phenomena for all layered, lithiated-TM-oxides, particularly when operated at high voltages. Therefore, continued efforts to understand this complex class of cathodes are encouraged as they may uncover further information and advances relevant to the field of Li-ion as a whole.

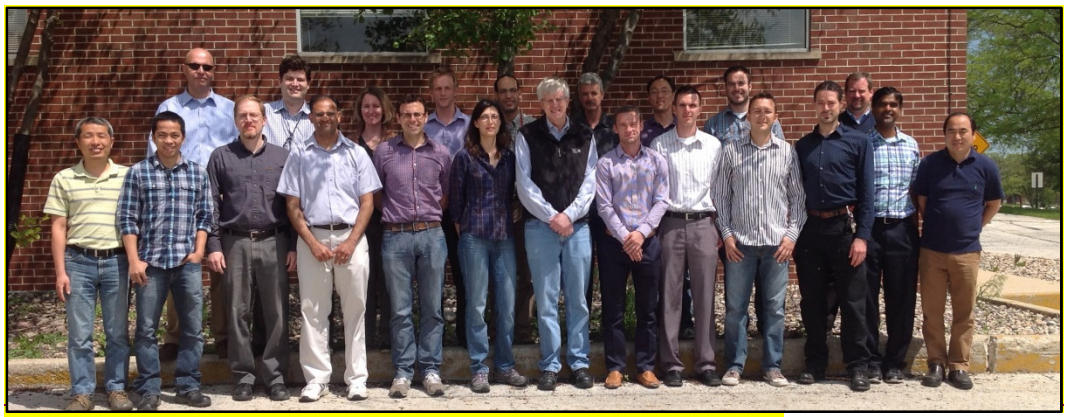

~~**Figure 15**—Voltage fade team (partial) at Argonne National Laboratory.~~

Biographies

Jason R. Croy received his Ph.D. in physics from the University of Central Florida. He is currently a materials scientist ~~in~~ at Argonne National Laboratory~~'s Electrochemical Energy Storage Department where his work focuses on design and synthesis of high-energy Li-ion materials with an emphasis on understanding atomic-scale processes through advanced characterization~~.

Mahalingam Balasubramanian received a Ph.D. in physics from the University of Connecticut. He is currently a physicist at the Advanced Photon Source in Argonne National Laboratory. ~~He is involved in the general operation, maintenance, and user support of Sector 20 X-ray beamlines. His personal research centers on the use of synchrotron techniques to investigate advanced and technologically important materials.~~

Kevin G. Gallagher received a Ph.D. in chemical engineering from the Georgia Institute of Technology. He is currently a chemical engineer ~~in the Electrochemical Energy Storage Department~~ at Argonne National Laboratory. ~~Kevin's work focuses on electrochemical characterization, materials development, techno-economic analyses, and continuum-scale modeling of electrochemical energy storage and conversion systems.~~

Anthony K. Burrell
Anthony K. Burrell received a Ph.D. in chemistry from the University of Auckland, New Zealand. He is currently the Head of the Electrochemical Energy Storage Department at Argonne National Laboratory.

Acknowledgements
Support from the Vehicle Technologies Program, Hybrid and Electric Systems, David Howell, Peter Faguy, and Tien Duong at the U.S. Department of Energy, Office of Energy Efficiency and Renewable Energy, is gratefully acknowledged. Use of Sector 20 facilities at the Advanced Photon Source, computer allocations at the LCRC (ANL), NERSC and EMSL (PNNL), and support from the members of the Voltage Fade team are gratefully acknowledged. This work was performed under the auspices of the DOE Office of Vehicle Technologies, under Contract No. DE-AC02-06CH11357.

References

(1) Gallagher, K. G.; Goebel, S.; Greszler, T.; Mathias, M.; Oelerich, W.; Eroglu, D.; Srinivasan, V. Quantifying the promise of Li-air batteries for electric vehicles. *Energy Environ. Sci.* **2014**, *7*, 1555-1563.

(2) Croy, J. R.; Gallagher, K. G.; Balasubramanian, M.; Long, B. R.; Thackeray, M. M. Quantifying Hysteresis and Voltage Fade in xLi_2MnO_3•$LiMn_{0.5}Ni_{0.5}O_2$ Electrodes as a Function of Li_2MnO_3 Content. *J. Electrochem. Soc.* **2014**, *161*, A318-A325.

(3) Croy, J. R.; Abouimrane, A.; Zhang, Z. C. Next-generation Li-ion batteries: The promise of near-term advancements. *MRS Bull.* **2014**, *39*, 407-415.

(4) Lu, Z. H.; Dahn, J. R. Understanding the anomalous capacity of $Li/Li[Ni_xLi_{1/3-2x/3}Mn_{2/3-x/3}]O_2$ cells using in situ X-ray diffraction and electrochemical studies. *J. Electrochem. Soc.* **2002**, *149*, A815-A822.

(5) Armstrong, A. R.; Holzapfel, M.; Novak, P.; Johnson, C. S.; Kang, S. H.; Thackeray, M. M.; Bruce, P. G. Demonstrating oxygen loss and associated structural reorganization in the Li battery cathode $Li[Ni_{0.2}Li_{0.2}Mn_{0.6}]O_2$. *J. Am. Chem. Soc.* **2006**, *128*, 8694-8698.

(6) Meng, Y. S.; Ceder, G.; Grey, C. P.; Yoon, W. S.; Jiang, M.; Breger, J.; Shao-Horn, Y. Cation ordering in layered O3 $Li[Ni_xLi_{1/3-2x/3}Mn_{2/3-x/3}]O_2$ ($0 <= x <= 1/2$) compounds. *Chem. Mater.* **2005**, *17*, 2386-2394.

(7) Jarvis, K. A.; Deng, Z. Q.; Allard, L. F.; Manthiram, A.; Ferreira, P. J. Atomic Structure of a Li-Rich Layered Oxide Material for Li-Ion Batteries: Evidence of a Solid Solution. *Chem. Mater.* **2011**, *23*, 3614-3621.

(8) Long, B. R.; Croy, J. R.; Dogan, F.; Suchomel, M. R.; Key, B.; Wen, J. G.; Miller, D. J.; Thackeray, M. M.; Balasubramanian, M. Effect of Cooling Rates on Phase Separation in $0.5Li_2MnO_3$•$0.5LiCoO_2$ Electrode Materials for Li-Ion Batteries. *Chem. Mater.* **2014**, *26*, 3565-3572.

(9) Bareno, J.; Balasubramanian, M.; Kang, S.H.; Wen, J.G.; Lei, C.H.; Pol, S.V.; Petrov, I.; Abraham, D.P.; Long-Range and Local Structure in the Layered Oxide $Li_{1.2}Co_{0.4}Mn_{0.4}O_2$. *Chem. Mat.* **2011**, 23, 2039-2050.

(10) Jiang, M.; Key, B.; Meng, Y. S.; Grey, C. P. Electrochemical and Structural Study of the Layered, "Li-Excess" Li-Ion Battery Electrode Material $Li[Li_{1/9}Ni_{1/3}Mn_{5/9}]O_2$. *Chem. Mater.* **2009**, *21*, 2733-2745.

(11) Jain, G. R.; Yang, J. S.; Balasubramanian, M.; Xu, J. J. Synthesis, electrochemistry, and structural studies of Li intercalation of a nanocrystalline Li_2MnO_3-like compound. *Chem. Mater.* **2005**, *17*, 3850-3860.

(12) Kan, Y.; Hu, Y.; Croy, J. R.; Ren, Y.; Sun, C.-J.; Heald, S. M.; Bareno, J.; Bloom, I.; Chen, Z. H. Formation of Li_2MnO_3 investigated by in situ synchrotron probes. *J. Power Sources* **2014**, *266*, 341-346.

(13) Croy, J. R.; Park, J. S.; Dogan, F.; Johnson, C. S.; Key, B.; Balasubramanian, M. First-Cycle Evolution of Local Structure in Electrochemically Activated Li_2MnO_3. *Chem. Mater.* **2014**, *26*, 7091-7098.

(14) Croy, J. R.; Iddir, H.; Gallagher, K. G.; Johnson, C.; Benedek, R.; Balasubramanian, M. First-charge instabilities of layered-layered Li-ion-battery materials. *Phys. Chem. Chem. Phys.* **2015**, DOI: 10.1039/c5cp02943k.

(15) Dogan, F.; Croy, J. R.; Balasubramanian, M.; Slater, M. D.; Iddir, H.; Johnson, C. S.; Vaughey, J. T.; Key, B. Solid State NMR Studies of Li_2MnO_3 and Li-Rich Cathode Materials: Proton Insertion, Local Structure, and Voltage Fade. *J. Electrochem. Soc.* **2015**, *162*, A235-A243.

(16) Gallagher, K. G.; Croy, J. R.; Balasubramanian, M.; Bettge, M.; Abraham, D. P.; Burrell, A. K.; Thackeray, M. M. Correlating hysteresis and voltage fade in Li- and manganese-rich layered transition-metal oxide electrodes. *Electrochem. Commun.* **2013**, *33*, 96-98.

(17) Croy, J. R.; Gallagher, K. G.; Balasubramanian, M.; Chen, Z. H.; Ren, Y.; Kim, D.; Kang, S. H.; Dees, D. W.; Thackeray, M. M. Examining Hysteresis in Composite xLi_2MnO_3•$(1-x)LiMO_2$ Cathode Structures. *J. Phys. Chem. C* **2013**, *117*, 6525-6536.

(18) Dogan, F.; Long, B. R.; Croy, J. R.; Gallagher, K. G.; Iddir, H.; Russell, J. T.; Balasubramanian, M.; Key, B. Re-entrant Li Local Environments and Defect Driven Electrochemistry of Li- and Mn-Rich Li-Ion Battery Cathodes. *J. Am. Chem. Soc.* **2015**, *137*, 2328-2335.

(19) Kim, S.; Ma, X. H.; Ong, S. P.; Ceder, G. A comparison of destabilization mechanisms of the layered Na_xMO_2 and Li_xMO_2 compounds upon alkali de-intercalation. *Phys. Chem. Chem. Phys.* **2012**, *14*, 15571-15578.

(20) Mohanty, D.; Li, J.; Abraham, D.; Huq, A.; Payzant, E.A.; Wood, D.L.; Daniel, C. Unraveling the Voltage-Fade Mechanism in High-Energy-Density Lithium-Ion Batteries *Chem. Mat.* **2014**, 26, 6272-6280.

(21) Genovois, C.; Koga, H.; Croguenedd, L.; Menterier, M.; Delmas, C.; Weill, F. Insight into the Atomic Structure of Cycled Lithium-Rich Layered Oxide Li1.20Mn0.54Co0.13Ni0.13O2 Using HAADF STEM and Electron Nanodiffraction. *Phys. Chem. C* **2015**, 119, 75-83.

(22) Sathiya, M.; Abakumov, A.M.; Foix, D.; Rousse, G.; Ramesha, K.; Saubanere, M.; Doublet, M.L.; Vezin, H.; Laisa, C.P.; Prakash, A.S.; Gonbeau, D.; Van Tendeloo, G.; Tarascon, J-M. Origin of Voltage Decay in High-Capacity Layered Oxide Electrodes. *Nat. Mat.* **2015**, 14, 230-238.

(23) Karan, N. K.; Abraham, D. P.; Balasubramanian, M.; Furczon, M. M.; Thomas, R.; Katiyar, R. S. Morphology, Structure, and Electrochemistry of Solution-Derived $LiMn_{0.5-x}Cr_{2x}Ni_{0.5-x}O_2$ for Li-Ion Cells. *J. Electrochem. Soc.* **2009**, *156*, A553-A562.

(24) Iddir, H.; Key, B.; Dogan, F.; Russell, J. T.; Long, B. R.; Bareno, J.; Croy, J. R.; Benedek, R. Pristine-state structure of Li-ion-battery cathode material $Li_{1.2}Mn_{0.4}Co_{0.4}O_2$ derived from NMR bond pathway analysis. *J. Mater. Chem. A* **2015**, *3*, 11471-11477.

(25) Bloom, I.; Trahey, L.; Abouimrane, A.; Belharouak, I.; Zhang, X. F.; Wu, Q. L.; Lu, W. Q.; Abraham, D. P.; Bettge, M.; Elam, J. W.; Meng, X. B.; Burrell, A. K.; Ban, C. M.; Tenent, R.; Nanda, J.; Dudney, N. Effect of interface modifications on voltage fade in $0.5Li_2MnO_3 \bullet 0.5LiNi_{0.375}Mn_{0.375}CO_{0.25}O_2$ cathode materials. *J. Power Sources* **2014**, *249*, 509-514.

(26) Lee, E.; Park, J. S.; Wu, T. P.; Sun, C. J.; Kim, H.; Stair, P. C.; Lu, J.; Zhou, D. H.; Johnson, C. S. Role of Cr^{3+}/Cr^{6+} redox in chromium-substituted $Li_2MnO_3 \bullet LiNi_{1/2}Mn_{1/2}O_2$ layered composite cathodes: electrochemistry and voltage fade. *J. Mater. Chem. A* **2015**, *3*, 9915-9924.

(27) Lee, E.; Koritala, R.; Miller, D. J.; Johnson, C. S. Aluminum and Gallium Substitution into $0.5Li_2MnO_3 \bullet 0.5LiNi_{0.375}Mn_{0.375}Co_{0.25}O_2$ Layered Composite and the Voltage Fade Effect. *J. Electrochem. Soc.* **2015**, *162*, A322-A329.

(28) Bettge, M.; Li, Y.; Gallagher, K.; Zhu, Y.; Wu, Q. L.; Lu, W. Q.; Bloom, I.; Abraham, D. P. Voltage Fade of Layered Oxides: Its Measurement and Impact on Energy Density. *J. Electrochem. Soc.* **2013**, *160*, A2046-A2055.
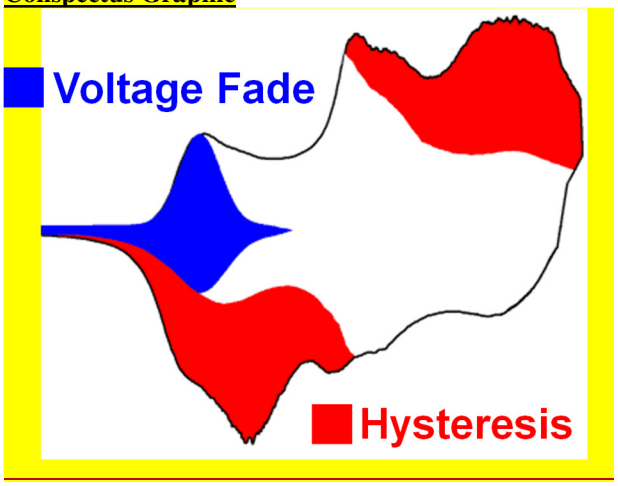
Conspectus Graphic